TU Delft

Delft University of Technology

Using advanced adaptive cruise control systems to reduce congestion at sags

An evaluation based on microscopic traffic simulation

Goñi-Ros, Bernat; Schakel, Wouter J.; Papacharalampous, Alexandros E.; Wang, Meng; Knoop, Victor L.; Sakata, Ichiro; van Arem, Bart; Hoogendoorn, Serge P.

DOI
10.1016/j.trc.2019.02.021

Publication date
2019

Document Version
Final published version

Published in
Transportation Research Part C: Emerging Technologies

Citation (APA)
Goñi-Ros, B., Schakel, W. J., Papacharalampous, A. E., Wang, M., Knoop, V. L., Sakata, I., van Arem, B., & Hoogendoorn, S. P. (2019). Using advanced adaptive cruise control systems to reduce congestion at sags: An evaluation based on microscopic traffic simulation. *Transportation Research Part C: Emerging Technologies*, *102*, 411-426. https://doi.org/10.1016/j.trc.2019.02.021

Important note
To cite this publication, please use the final published version (if applicable).
Please check the document version above.

Copyright
Other than for strictly personal use, it is not permitted to download, forward or distribute the text or part of it, without the consent of the author(s) and/or copyright holder(s), unless the work is under an open content license such as Creative Commons.

Takedown policy
Please contact us and provide details if you believe this document breaches copyrights.
We will remove access to the work immediately and investigate your claim.

This work is downloaded from Delft University of Technology.
For technical reasons the number of authors shown on this cover page is limited to a maximum of 10.

Green Open Access added to TU Delft Institutional Repository

'You share, we take care!' – Taverne project

https://www.openaccess.nl/en/you-share-we-take-care

Otherwise as indicated in the copyright section: the publisher is the copyright holder of this work and the author uses the Dutch legislation to make this work public.

Transportation Research Part C 102 (2019) 411–426

Contents lists available at ScienceDirect

Transportation Research Part C

journal homepage: www.elsevier.com/locate/trc

Using advanced adaptive cruise control systems to reduce congestion at sags: An evaluation based on microscopic traffic simulation

Bernat Goñi-Ros[a], Wouter J. Schakel[a], Alexandros E. Papacharalampous[b], Meng Wang[a], Victor L. Knoop[a,*], Ichiro Sakata[c], Bart van Arem[a], Serge P. Hoogendoorn[a]

[a] Delft University of Technology, Faculty of Civil Engineering and Geosciences, Department of Transport and Planning, Stevinweg 1, 2628 CN Delft, The Netherlands
[b] AETHON Engineering Consultants, Emmanouil Benaki 25, 106 78 Athens, Greece
[c] Toyota Motor Europe, Technical Center, Hoge Wei 33, 1930 Zaventem, Belgium

ARTICLE INFO

Keywords:
Sag vertical curve
Freeway capacity
Adaptive Cruise Control
Traffic management
Microscopic traffic simulation

ABSTRACT

Sags are roadway sections along which the gradient increases gradually in the direction of traffic. Sags are generally bottlenecks in freeway networks. Previous research suggests that traffic management measures using advanced Adaptive Cruise Control (ACC) systems could reduce congestion on freeways, but little is known about their potential effectiveness at sags. This article evaluates the effectiveness of a basic ACC system (B-ACC) and two advanced ACC systems – Traffic State-Adaptive ACC (TSA-ACC) and Cooperative ACC (C-ACC) – in mitigating congestion at sags. TSA-ACC adapts the ACC parameters to the macroscopic traffic state estimated by the vehicle itself. C-ACC uses information of other vehicles in the surroundings to adjust its accelerations. Results are obtained using microscopic traffic simulations with different penetration rates. They show that, under high-demand conditions, congestion decreases with increasing percentage of vehicles equipped with B-ACC. With high penetration rates (75% and above), traffic no longer becomes congested at the sag. Moreover, the results show that TSA-ACC and C-ACC reduce congestion more than B-ACC, mainly because they increase the queue discharge capacity of the sag. The two advanced ACC systems prevent the formation of congestion at the sag at lower penetration rates than B-ACC. TSA-ACC is the most effective system. C-ACC is only more effective than B-ACC in scenarios with 20% penetration rate or higher; below that, connectivity between equipped vehicles is too low. Our findings show the potential of using advanced ACC systems to mitigate congestion at sags and indicate some challenges of this traffic management approach.

1. Introduction

Sag vertical curves (or sags) are roadway sections along which the gradient increases gradually in the direction of traffic. In

* Corresponding author.
E-mail addresses: b.goniros@tudelft.nl (B. Goñi-Ros), w.j.schakel@tudelft.nl (W.J. Schakel), a.papacharalampous@aethon.gr (A.E. Papacharalampous), m.wang@tudelft.nl (M. Wang), v.l.knoop@tudelft.nl (V.L. Knoop), ichiro.sakata@toyota-europe.com (I. Sakata), b.vanarem@tudelft.nl (B. van Arem), s.p.hoogendoorn@tudelft.nl (S.P. Hoogendoorn).

https://doi.org/10.1016/j.trc.2019.02.021
Received 28 September 2018; Received in revised form 26 February 2019; Accepted 28 February 2019
0968-090X/ © 2019 Elsevier Ltd. All rights reserved.

general, they provide a transition between two sloped roadway sections, allowing vehicles to negotiate the change in gradient in a gradual way. Empirical observations show that sags can be bottlenecks in freeway networks (Koshi et al., 1992; Patire and Cassidy, 2011; Xing et al., 2014; Sun et al., 2018). The main reason is that most drivers unintentionally change their longitudinal driving behavior when they drive through this type of freeway sections (Goñi-Ros et al., 2014a). More specifically, they reduce their free speed (Brilon and Bressler, 2004) and keep longer headways than expected (Koshi, 2003), which leads to a local decrease in freeway capacity (Okamura et al., 2000). Consequently, traffic becomes congested at lower flow rates (typically, 10–25% lower) than in constant-gradient freeway sections (Koshi et al., 1992; Patire and Cassidy, 2011). In some countries (such as Japan), sags are one of the most frequent type of freeway bottlenecks, causing a large number of traffic jams throughout the year (Hatakenaka et al., 2006). For this reason, various traffic management measures have been proposed in recent years to prevent the formation of congestion at sags or to reduce its severity (Sun et al., 2018; Hatakenaka et al., 2006; Sato et al., 2009).

Adaptive Cruise Control (ACC) systems are in-vehicle control systems that automatically regulate the longitudinal vehicle acceleration. These systems typically operate in two modes: cruising or following mode. In cruising mode, they regulate acceleration so as to reach/maintain a free speed defined by the user. In following mode, they regulate acceleration so as to reach/maintain a user-defined time gap. Basic ACC systems take control actions based on information from on-board sensors (e.g., radar). Furthermore, there are advanced ACC systems that also take into account information sent by other vehicles or traffic control centers. Previous research suggests that traffic management measures using advanced ACC systems could mitigate congestion at various types of freeway bottlenecks (Kesting et al., 2008; Shladover et al., 2012; Roncoli et al., 2016). However, little is known about the effectiveness of these systems in reducing congestion at sags.

This article evaluates the effectiveness of a basic ACC (B-ACC) system and two advanced ACC systems – Traffic State-Adaptive ACC (TSA-ACC) and Cooperative ACC (C-ACC) – in mitigating congestion at freeway sags. Our basic ACC controller is a non-linear state-feedback controller that applies the constant time-gap policy and has an emergency-braking mode. It was developed based on the working principles of the ACC controllers proposed by Shladover et al. (2012) and Moon et al. (2009), and the analysis of the behavior of a model prective ACC controller (Wang et al., 2014a). The TSA-ACC and C-ACC controllers are extensions of the B-ACC controller. The TSA-ACC system's adaptation to the current traffic state is inspired by the active congestion avoidance presented in Kesting et al. (2008). C-ACC adds anticipative behavior to the B-ACC system and is inspired by Schakel et al. (2010). Previous research suggests that basic ACC systems could potentially increase the capacity of sags and, thus, reduce traffic congestion (Ozaki, 2003). The TSA-ACC and C-ACC systems may reduce congestion to a greater extent than the basic ACC system due to their additional capabilities.

The main objective of this article is to evaluate the potential effectiveness of these types of ACC systems – particularly the two advanced systems – in mitigating congestion at freeway sags. Note that the study focuses on the potential impacts of the ACC systems on traffic flow dynamics rather than on their technical characteristics (which may play an important role, e.g., slow responses could lead to large gaps and low capacities). Optimization of the performance of the ACC systems is also beyond the scope of the study. The evaluation is done through microscopic traffic simulation. The simulated network consists of a three-lane freeway stretch containing a sag. The network has a similar layout to that of a section of the Tomei Expressway (Japan) where traffic often becomes congested. Empirical traffic data from an episode of congestion at this site are available (Patire and Cassidy, 2011; Goñi-Ros et al., 2014a) and have been used to calibrate a microscopic traffic model consisting of a car-following model that takes into account the effect of vertical curves and a lane-changing model (Goñi-Ros et al., 2016a). The systems are tested in various scenarios with different penetration rates of ACC-equipped vehicles. The effectiveness of each ACC system at each penetration rate is evaluated by comparing the Average Travel Time (ATT) and the Average Vehicle Delay (AVD) with scenarios with no equipped vehicles. Preliminary results were presented at a conference, see Papacharalampous et al. (2015). This paper presents an extended version of the research reported in Papacharalampous et al. (2015), with more realistic simulation scenarios (multi-lane freeway and presence of trucks), improved ACC controllers, and an analysis of the influence of the penetration rate on controller performance.

The paper begins with a literature review on the characteristics of traffic flow at sags and the use of ACC systems in freeway traffic management (Section 2). Next, Section 3 presents the three ACC controllers, focusing on their working principles and mathematical formulation. The setup of the simulation study that was performed to evaluate the effectiveness of the three ACC systems is described in Section 4. Finally, Sections 5 and 6 report the results of the evaluation and present the conclusions of this research, respectively.

2. Background

2.1. Traffic dynamics at freeway sags

Empirical observations show that most drivers change their longitudinal driving behavior when they go through freeway sags. More specifically, their free speed decreases (Brilon and Bressler, 2004; Furuichi et al., 2003), and they keep longer gaps than expected given their speed (Koshi, 2003). These behavioral changes are generally unintentional: they appear to be caused mainly by inadequate acceleration behavior (Yoshizawa et al., 2012). However, in the case of trucks the cause may sometimes be related to insufficient acceleration capability (Laval, 2009). The special characteristics of longitudinal driving behavior at freeway sags have crucial implications for traffic dynamics. Most importantly, they reduce the free-flow capacity of the freeway, as explained by Jin (2018). Indeed, previous empirical research shows that the free-flow capacity of sags is 10–25% lower than that of flat freeway sections having the same number of lanes (Koshi et al., 1992; Okamura et al., 2000). As a result, traffic often breaks down at sags under high-demand conditions (Koshi et al., 1992; Patire and Cassidy, 2011; Sun et al., 2018). It should be noted that, although the presence of heavy vehicles has a negative impact on the capacity of freeway sags (Brilon and Bressler, 2004; Okamura et al., 2000),

congestion also occurs when traffic is composed mainly of passenger cars (Furuichi et al., 2003).

Typically, traffic congestion forms at sags in two phases (Koshi et al., 1992; Patire and Cassidy, 2011). Firstly, traffic becomes congested on the median lane. The main reason why this lane is the first to become congested is that, under high-demand and uncongested-traffic conditions, flow tends to be higher (and closer to the free-flow capacity) there than on the other lanes (Xing et al., 2014; Hatakenaka et al., 2006). Secondly, congestion spreads to the other lanes because some vehicles move from the median lane to these lanes in order to avoid having to slow down (Patire and Cassidy, 2011; Hatakenaka et al., 2006). When the flow on these lanes exceeds their free-flow capacity, traffic becomes congested there as well. The formation of traffic congestion on all lanes significantly reduces the total outflow (due to the congestion-induced capacity drop (Hall and Agyemang-Duah, 1991; Jin, 2018; Yuan et al., 2018)) and causes the formation of a queue (Koshi et al., 1992; Patire and Cassidy, 2011). In general, the head of the queue stays on the first 0.5–1.0 km downstream of the location along the sag that has the lowest altitude (Sun et al., 2018; Brilon and Bressler, 2004). Stop-and-go waves emerge frequently within queues at sags (Goñi-Ros et al., 2014a; Zheng et al., 2011).

2.2. ACC applications in freeway traffic management

It is generally accepted that basic ACC systems alone have only marginal effects on traffic flow (Shladover et al., 2012; VanderWerf et al., 2001). Theoretically, they could increase freeway capacity if they operated with shorter time gaps than those kept by human drivers. However, with such settings, basic ACC systems make it difficult for traffic to achieve string stability, which limits the potential capacity gain. Extensions of the basic ACC concept specifically designed to mitigate congestion have been proposed and tested, e.g., ACC systems with adaptive driving strategies (Kesting et al., 2008), cooperative ACC systems (Shladover et al., 2012; VanderWerf et al., 2001; Wang et al., 2014b; Jin and Orosz, 2014; Xiao et al., 2018), and ACC systems integrated with roadside traffic control measures (Roncoli et al., 2016; Ioannou et al., 2007; Wang et al., 2016; Scarinci et al., 2015). The scientific literature suggests that these advanced ACC systems can help to mitigate congestion in freeways.

An advanced ACC system with adaptive driving strategy is reported by Kesting et al. (2008). The Intelligent Driver Model (IDM) (Treiber et al., 2000) is used to model ACC systems. The adaptive strategy entails dynamically changing the time gap and maximum acceleration parameters of the IDM depending on whether the ACC-equipped vehicle is approaching, inside or leaving a traffic jam. For instance, decreasing the time gap and increasing the maximum acceleration when leaving the jam effectively increases the queue discharge rate, which reduces congestion. The adaptive driving strategy presented by Kesting et al. (2008) is based on a decentralized traffic state-estimation algorithm that uses on-board measurements made by the ACC system.

Cooperative ACC (C-ACC) systems are enhanced versions of the basic ACC concept that use information sent by the platoon leader, multiple predecessors or the direct predecessor in addition to on-board measurements to determine the vehicle acceleration. This extra information is exchanged by means of vehicle-to-vehicle (V2V) communication technology. The use of C-ACC systems leads to enhanced string stability; consequently, vehicles equipped with C-ACC can maintain shorter time headways than vehicles equipped with basic ACC systems without disrupting traffic, which increases freeway capacity (Shladover et al., 2012; Van Arem et al., 2006; Ploeg et al., 2014b; Xiao et al., 2018; Liu et al., 2018). In addition, as a result of their ability to anticipate downstream traffic conditions, C-ACC systems can increase queue discharge flows (Wang et al., 2014b). The main limitation of C-ACC systems is that equipped vehicles need to follow each other in a platoon in order to enable connectivity, which is unlikely to occur at low market penetration rates. There are more options for control if one includes lane changing as well in the control scheme (Liu et al., 2018). Besides, recent findings by Xiao et al. (2018) show the importance of switching between modes of the C-ACC for the capacity. The human factors are also explicitly studied by Jin and Orosz (2018), who developed a C-ACC controller based on the positions of various vehicles upstream, dampening out disturbances.

Another type of ACC application is the integration with traffic control systems via infrastructure-to-vehicle (I2V) communication. Some studies present systems that integrate variable speed limits (VSL) with ACC systems (Roncoli et al., 2016; Ioannou et al., 2007; Wang et al., 2016). All these systems have a hierarchical architecture where the higher-level traffic controller regulates speeds using VSL signs, while ACC systems control accelerations using the propulsion and brake systems of the vehicles. ACC-equipped vehicles receive VSL commands from the traffic controller and use them as variable parameters for the local vehicle controller. A further extension of the concept is that the ACC parameters can be adapted (Spiliopoulou et al., 2017). Based on this principle, the same authors present an algorithm to change car-following parameters dynamically based on the traffic state (Spiliopoulou et al., 2018). In this paper, they present the concept where just upstream of a speed increase the headway setting is lowered in order to increase the queue discharge rate. Simulation results show that integrating traffic control measures with ACC systems leads to better performance than using only decentralized ACC systems (Wang et al., 2016).

This article aims to evaluate the effectiveness of a basic ACC system and two advanced ACC systems (a system with adaptive diving strategy and a cooperative system) in reducing congestion at freeway sags. Note that, in the case of sags, basic ACC systems are expected to increase the capacity of the bottleneck and, thus, to reduce congestion (Ozaki, 2003; Goñi-Ros et al., 2016b). The main reason is that the acceleration behavior of vehicles equipped with these systems is not affected by the freeway slope, unlike that of human-driven vehicles. Therefore, even if the basic ACC systems operate with normal time headways (thus guaranteeing string stability), equipped vehicles keep shorter gaps than human drivers, which increases the sag capacity. The two advanced ACC systems are expected to reduce congestion further than the basic ACC system due to their additional features.

3. Controllers

This section describes the characteristics of the three ACC systems that will be evaluated and provides the mathematical

formulation of their control laws. The ACC systems are: Basic ACC (Section 3.1), Traffic State-Adaptive ACC (Section 3.2) and Cooperative ACC (Section 3.3). The control law is the rule used to determine the longitudinal acceleration of an equipped vehicle i in every control time step κ ($\kappa = 0, 1, 2, \ldots, \kappa_F$, where $\kappa = 0$ is the initial control time step, when vehicle i enters the network, and $\kappa = \kappa_F$ is the final control time step, when vehicle i exits the network) given some input data. We assume that the ACC systems apply the vehicle accelerations determined by their control laws in such a way that acceleration is constant over the duration of every control time step. The control time step length is denoted by $\Delta\kappa$.

3.1. Basic ACC

The B-ACC controller is a non-linear state-feedback controller that applies the constant time-gap (CTG) policy (Shladover et al., 2012; Van Arem et al., 2006). The controller adjusts the acceleration of the vehicle so as to keep its speed close to a certain gap-dependent speed value, similarly to Shladover et al. (2012). In addition, however, our B-ACC controller reacts to the approach rate divided by the gap, making the vehicle decelerate considerably faster when it approaches the leading vehicle and the distance between them is short. This B-ACC controller was developed based on the analysis of the behavior of a flexible model predictive ACC controller (Wang et al., 2014a), although its control law is formulated simply in an efficient state-feedback fashion. The control law that regulates the acceleration of a vehicle i equipped with the B-ACC system in time step κ is as follows:

- If $s_i(\kappa) \leqslant r_{B-ACC}$:

$$a_i^{B-ACC}(\kappa) = K_1 \cdot (V_i^{B-ACC}(\kappa) - v_i(\kappa)) + K_2 \cdot \frac{\Delta v_i(\kappa)}{s_i(\kappa)} \tag{1}$$

- If $s_i(\kappa) > r_{B-ACC}$:

$$a_i^{B-ACC}(\kappa) = K_1 \cdot (V_i^{B-ACC}(\kappa) - v_i(\kappa)) \tag{2}$$

In Eqs. (1) and (2), v_i denotes the speed of the controlled vehicle, s_i denotes the distance gap, and Δv_i denotes the relative speed to the predecessor ($\Delta v_i = v_{i-1} - v_i$). We assume that on-board sensors continuously monitor these variables and provide the information to the B-ACC controller without delay and free of errors. Furthermore, in Eqs. (1) and (2), K_1 and K_2 are control gains, and r_{B-ACC} is the on-board sensor detection range. Radar-based systems generally have a r_{B-ACC} of around 150 m. Finally, V_i^{B-ACC} is a gap-dependent target speed that is calculated as follows:

$$V_i^{B-ACC}(s_i) = \min\left(\frac{s_i(\kappa) - s_s}{T_d}, v_d\right) \tag{3}$$

where: parameter s_s is the distance gap at standstill; and parameters T_d and v_d are the desired time gap and the desired free speed, respectively, whose values are defined by the user. Note that, with the control parameter values used in this study (see Section 4.4), V_i^{B-ACC} always equals v_d if $s_i > r_{B-ACC}$. This implies that the right-hand expression of Eq. (2) could be rewritten as $K_1 \cdot (v_d - v_i(\kappa))$.

The B-ACC controller works as follows. When there is no vehicle within range ($s_i > r_{B-ACC}$), it regulates the acceleration in such a way that the vehicle will move at the desired free speed v_d (see Eqs. (2) and (3)). When the preceding vehicle is within range ($s_i \leqslant r_{B-ACC}$), the first term of the control law regulates the acceleration so as to make the vehicle move at a gap-dependent speed V_i^{B-ACC} (see Eq. (1)), which is proportional to the distance to the predecessor but never higher than v_d (see Eq. (3)). The second term of the control law increases the deceleration rate when the vehicle approaches its leader with short gaps (see Eq. (1)). The latter term differentiates our B-ACC control law from those of traditional (linear) ACC controllers (e.g., Shladover et al. (2012)). As mentioned above, this term was included in the control law based on the analysis of the behavior of a model predictive ACC controller (Wang et al., 2014a).

It should be noted that the B-ACC control law is subject to the following two constraints:

- Non-collision constraint:

$$TTC_i(\kappa) \geqslant TTC_{min} \text{ and } s_i(\kappa) \geqslant s_{min}, \forall \kappa \tag{4}$$

where TTC_{min} and s_{min} are thresholds; and TTC_i denotes the time-to-collision of vehicle i (i.e., the time needed for this vehicle to collide with its predecessor if both vehicles would keep moving at their current speed), which can be calculated as follows:

$$TTC_i(\kappa) = \frac{s_i(\kappa)}{v_i(\kappa) - v_{i-1}(\kappa)} \tag{5}$$

- Admissible acceleration range:

$$a_{min} \leqslant a_i^{B-ACC}(\kappa) \leqslant a_{max}, \forall \kappa \tag{6}$$

The practical implementation of these constraints is as follows. In every time step κ, the controller checks whether the time-to-collision (TTC_i) is lower than the minimum threshold TTC_{min} or the distance gap (s_i) is lower than the minimum threshold s_{min} (see Eq. (4)). If this is not the case, the controller determines the acceleration for the current time step using Eqs. (1) or (2). However, if $TTC_i < TTC_{min}$ or $s_i < s_{min}$, the controller applies emergency braking to avoid rear-end collisions, similarly to Moon et al. (2009). In emergency-braking mode, the vehicle acceleration is calculated using an alternative formula:

$$a_{emg,i}^{B-ACC}(\kappa) = \min\left(-\frac{\Delta v_i(\kappa)^2}{2 \cdot s_i(\kappa)}, K_1 \cdot (V_i^{B-ACC}(\kappa) - v_i(\kappa)) + K_2 \cdot \frac{\Delta v_i(\kappa)}{s_i(\kappa)}\right) \tag{7}$$

where the second argument of the min-function is the same expression used to calculate a_i^{B-ACC} in non-emergency conditions if the preceding vehicle is within range (see Eq. (1)).

After calculating the acceleration a_i^{B-ACC} via Eqs. (1), (2) or (7), the controller checks whether this acceleration is within the admissible range (see Eq. (6)). If the calculated acceleration is greater than the maximum threshold or lower than the minimum threshold, then the acceleration to be applied by the controller becomes a_{max} or a_{min}, respectively.

3.2. Traffic state-adaptive ACC

The TSA-ACC controller is an extension of the B-ACC controller (see Section 3.1) that was developed based on the concept of ACC for active congestion avoidance presented in Kesting et al. (2008). The TSA-ACC controller determines the acceleration of equipped vehicles based on slightly different formulas than those used by the B-ACC controller (Eqs. (1)–(3)) but subject to the same constraints (Eqs. (4)–(7)). It has two added features relative to the B-ACC controller. First, it estimates the traffic state (based on information provided by on-board sensors, which are the same used by the B-ACC controller). Second, it adjusts the value of control parameter T_d (desired time gap) based on the detected traffic state. Therefore, the TSA-ACC controller determines the vehicle acceleration ($a_i^{TSA-ACC}$) using the same formulas used to calculate a_i^{B-ACC} (Eqs. (1), (2) and (7)), but it calculates the gap-dependent target speed (variable V_i^{B-ACC} in Eqs. (1), (2) and (7)) in a slightly different way than the B-ACC controller does. The desired time gap is time-variant, i.e., $T_d = T_d(\kappa)$, thus:

$$V_i^{TSA-ACC}\left(s_i, T_d\right) = \min\left(\frac{s_i(\kappa) - s_s}{T_d(\kappa)}, v_d\right) \tag{8}$$

As mentioned above, the TSA-ACC controller incorporates a traffic state-estimation algorithm. This algorithm uses an exponential moving average (EMA) of the speed of the equipped vehicle to identify the traffic state. The EMA of the speed of vehicle i in control time step κ is calculated as follows:

$$v_{EMA,i}(\kappa) = (1 - \psi) \cdot v_i(\kappa) + \psi \cdot v_{EMA,i}(\kappa - 1) \tag{9}$$

with:

$$\psi = e^{-\Delta\kappa / T_r} \tag{10}$$

where T_r is the relaxation time parameter. Note that using the smoothing method implicitly induces delay in the estimation of vehicle speed and the larger the relaxation time T_r, the higher this delay effect.

Thus, the influence of speeds (v_i) older than $\kappa - [T_r/\Delta\kappa]$ control time steps on the moving average decreases exponentially (see Eqs. (9) and (10)). In the initial control time step ($\kappa = 0$), $v_{EMA,i}$ is initialized by setting its value to the current vehicle speed (i.e., $v_{EMA,i}(0) = v_i(0)$).

Once $v_{EMA,i}(\kappa)$ is known, the traffic state in control time step κ is determined using Algorithm 1.

Algorithm 1. Determining the traffic state of an equipped vehicle i in control time step κ.

1: **if** $v_{EMA,i}(\kappa) > v_{free}$ **then** vehicle i is in free-flow traffic.
2: **else if** $v_{EMA,i}(\kappa) < v_{cong}$ **then** vehicle i is in congested traffic.
3: **else if** $v_i(\kappa) - v_{EMA,i}(\kappa) < \lambda_a$ **then** vehicle i is approaching a traffic jam.
4: **else if** $v_i(\kappa) - v_{EMA,i}(\kappa) > \lambda_l$ **then** vehicle i is leaving a traffic jam.
5: **else** the traffic state is undefined.

Note that correlation between parameters λ_a and λ_l and parameter T_r is necessary for efficient traffic state estimation.

As mentioned above, the TSA-ACC controller adjusts the value of control parameter T_d (desired time gap) based on the detected traffic state. The adaptive driving strategy consists of:

- Increasing the value of parameter T_d to T_d^H when the vehicle approaches a traffic jam.
- Decreasing the value of parameter T_d to T_d^L when the vehicle is in congested traffic or passing the head of the queue.
- Setting the value of parameter T_d to its default value (T_d^0) if the vehicle is in free-flow traffic or the traffic state is undefined.

Note that the value of parameter T_d is adjusted gradually; more specifically, the controller changes the value of T_d linearly over a certain time period T_{imp}. Thus, during $T_{imp}/\Delta\kappa$ control time steps, the increase or decrease of T_d per time step is equal to:

$$\Delta T_d^+ = \frac{T_d^H - T_d'}{T_{imp}/\Delta\kappa} \quad \text{and} \quad \Delta T_d^- = \frac{T_d' - T_d^L}{T_{imp}/\Delta\kappa} \tag{11}$$

where T_d' is the value of parameter T_d right before the period when the value of T_d is changed starts. Note that if parameter T_d is in the process of being changed (to T_d^H, T_d^L or T_d^0), no other change is permitted.

The rationale underlying the adaptive driving strategy of the TSA-ACC controller is as follows. Two strategies are used to mitigate traffic congestion: (a) inflow control; and (b) increased queue discharge rate. First, when a controlled vehicle approaches a jam, the controller increases the desired time gap (T_d), which makes the vehicle decelerate. As a result, the following vehicles are forced to decelerate too, so the inflow into the jam decreases. Previous studies have shown that regulating inflow can reduce congestion at sags (Goñi-Ros et al., 2014b; GoñiRos et al., 2016b; Nezafat et al., 2018) and other types of bottlenecks (Carlson et al., 2011). Note however that for this type of strategy to work, the headway increase as well as the location of this increase play a role. For completeness, we include it in the TSA-ACC controller.

More important for the reduction in travel time is the second strategy: when a controlled vehicle is in congested traffic or leaving the queue, the controller reduces the desired time gap (T_d). As a result, the flow within the queue increases (since flow is equal to the inverse of the average time headway), particularly with high penetration rates of equipped vehicles. Note that increasing the outflow automatically reduces travel times (Papageorgiou et al., 2003). The increased outflow is caused by the shorter headway at the head of the queue. To ensure these headways are short, the headways are already shortened within the queue. Since the vehicles are ACC equipped, the short headways are not expected to cause collisions. However, it still could be uncomfortable and future improvement of this strategy could entail a robust head-of-queue detection algorithm, allowing for headways to be shortened only at the head of the queue.

3.3. Cooperative ACC

The C-ACC controller is another extension of the B-ACC controller (see Section 3.1). It determines the acceleration of equipped vehicles based on slightly different formulas than those used by the B-ACC controller (Eqs. (1)–(7)). The main added feature of the C-ACC controller relative to the B-ACC controller is that the formulas used to determine the vehicle acceleration in a particular control time step include a multi-anticipative term (Wilmink et al., 2007; Wang et al., 2014b). Therefore, vehicles equipped with the C-ACC system react to the driving behavior of other preceding vehicles equipped with that system besides the direct predecessor. In order to get information about the movement of other equipped vehicles, the C-ACC system receives information from the C-ACC systems installed in these vehicles through vehicle-to-vehicle (V2V) communication technology (we assume that information is received without delay and free of errors). Simultaneously, the C-ACC system sends information to other equipped vehicles. The typical communication range of V2V technology (r_{V2V}) is around 300 m. If there is no vehicle equipped with a C-ACC system downstream on the lane and within range, the C-ACC controller calculates the target acceleration exactly as the B-ACC controller does (see Eqs. (1) and (2)). However, if there are one or more equipped vehicles downstream on the lane and within range, then the vehicle acceleration is determined using a formula that includes the positions and speeds of these vehicles as variables. The system allows non-equipped vehicles to be present between the downstream equipped vehicles.

Let us define $N_c(\kappa)$ as the number of vehicles equipped with C-ACC that are downstream of the ego-vehicle and within the V2V communication range in a particular control time step (κ). Then, the acceleration control law for a vehicle i equipped with the C-ACC system is:

- If $N_c(\kappa) > 0$:

$$a_i^{C-AAC}(\kappa) = a_i^{B-AAC}(\kappa) + K_3 \cdot \sum_{j=1}^{N_c(\kappa)} \frac{v_j(\kappa) - v_i(\kappa)}{|x_j(\kappa) - x_i(\kappa)|} \tag{12}$$

- If $N_c(\kappa) = 0$:

$$a_i^{C-AAC}(\kappa) = a_i^{B-AAC}(\kappa) \tag{13}$$

where: j is an index assigned to every C-ACC-equipped vehicle located downstream and within range ($j = 1, 2, \ldots, N_c$); x_i and x_j denote the longitudinal positions along the road of vehicles i and j, respectively; K_3 is a control gain; and a_i^{B-AAC} is calculated using Eqs. (1)–(3).

Like the B-ACC controller, the C-ACC controller applies emergency braking if at any control time step κ the non-collision constraint (Eq. (4)) is not satisfied. In this case, however, the acceleration during emergency braking is calculated as follows:

$$a_{emg,i}^{B-ACC}(\kappa) = \min\left(-\frac{\Delta v_i(\kappa)^2}{2 \cdot s_i(\kappa)},\ K_1 \cdot (V_i^{B-ACC}(\kappa) - v_i(\kappa)) + K_2 \cdot \frac{\Delta v_i(\kappa)}{s_i(\kappa)} + K_3 \cdot \sum_{j=1}^{N_c(\kappa)} \frac{v_j(\kappa) - v_i(\kappa)}{|x_j(\kappa) - x_i(\kappa)|}\right) \tag{14}$$

where the second argument of the min-function is the same expression used to calculate a_i^{C-ACC} in non-emergency conditions if the distance to the preceding vehicle is shorter than r_{B-ACC} and $N_c > 0$ (see Eqs. (1) and (12)).

From Eq. (14) it follows that if there are no vehicles equipped with the C-ACC system downstream and within range (r_{V2V}), the

acceleration during emergency braking is calculated using the same formula used by the B-ACC and TSA-ACC controllers (Eq. (7)). Note that the admissible acceleration range constraint (see Eq. (6)) is enforced the same way the B-ACC and TSA-ACC controllers do (see Section 3.1).

The C-ACC control law is similiar to that of the cooperative ACC controller presented in Schakel et al. (2010). The main difference is that our C-ACC controller weights the contribution that other equipped vehicles have on the acceleration of the ego-vehicle using the distance between vehicles ($|x_j(\kappa) - x_i(\kappa)|$) instead of the order of the equipped vehicles along the roadway. Also, the cooperative ACC controller presented in Schakel et al. (2010) does not have an emergency-braking mode.

The reason why C-ACC is expected to reduce traffic congestion at sags to a greater extent than B-ACC is as follows. If a vehicle equipped with the C-ACC system detects a decrease (or increase) in speed of one or more equipped vehicles located downstream of its current position, then it decelerates (or accelerates) more than a vehicle equipped with the B-ACC system would do (see Eq. (12)). This additional amount of deceleration (or acceleration) is greater the closer the vehicle is to the other vehicles equipped with the C-ACC system detected downstream (Eq. (12)). Therefore, one can say that vehicles *anticipate* that they will have to decelerate (accelerate) as they move downstream. This implies that vehicles equipped with the C-ACC system will decelerate more smoothly when approaching a queue caused by a sag bottleneck than if they were equipped with the B-ACC system (thus they will disturb traffic to a lower extent). Also, they will accelerate faster when leaving the queue (thus increasing the queue discharge rate). Both effects can make the C-ACC system reduce congestion to a greater extent than the B-ACC system. Note that in this research we assume that the C-ACC system operates with the same desired time gap (T_d) than the B-ACC system (see also Section 4). Nevertheless, if the C-ACC system operated with shorter desired time gaps, it could potentially increase the capacity of the sag further (both in free-flow and congested traffic conditions), thus helping to reduce congestion to a greater extent.

4. Experimental setup

A microscopic traffic simulation study was carried out to assess the effectiveness of the controllers in reducing congestion at sags. This section describes the setup of the study.

4.1. Network

The simulated network is a freeway stretch that is 7 km long and contains a sag. The stretch has a constant-gradient downhill section that goes from location $x = 0$ to $x = 4.7$ km, a sag vertical curve that goes from $x = 4.7$ km to $x = 5.3$ km, and a constant-gradient uphill section that goes from $x = 5.3$ km to $x = 7.0$ km (see Fig. 1). The slopes of the constant-gradient downhill and uphill sections are -0.5% and $+2.5\%$, respectively. At the sag, the gradient increases linearly over distance. The vertical profile of the sag is similar to that of the Yamato sag of the Tomei Expressway (Japan), where traffic often becomes congested (Patire and Cassidy, 2011). The constant-gradient downhill section is quite long; this is necessary to guarantee that, if traffic becomes congested at the sag, the queue will not spill back to the network entry point. The freeway stretch has three lanes (median, center and shoulder lanes), as in the Yamato sag, and it has no ramps nor horizontal curves. The speed limit is assumed to be 100 km/h on the whole stretch, i.e. the regular speed limit on Japanese freeways.

4.2. Traffic demand

The simulation period is 2500 s (41.67 min). Initially, there are no vehicles in the network. The total traffic demand (i.e., the total flow on all lanes at point $x = 0$) changes over time as shown in Fig. 2. The traffic demand is distributed over the three lanes at the upstream boundary point according to the lane flow distribution model proposed by Hong and Oguchi (2008), which is calibrated for Japanese freeways. This model assumes that distribution is class-specific (it considers two vehicle classes, namely trucks and passenger cars) and depends on the total demand and truck percentage. In this research, lane flow distribution was assumed to be constant over time and was calculated for the highest level of demand given as input (5200 veh/h).

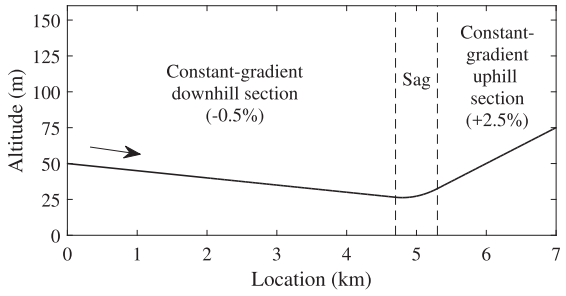

Fig. 1. Vertical alignment of the simulated freeway stretch.

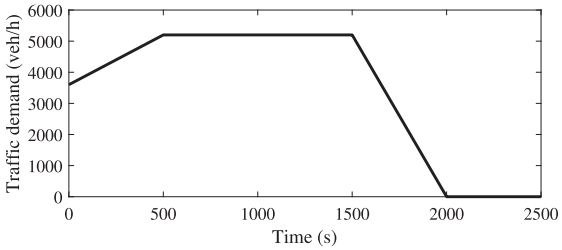

Fig. 2. Total traffic demand over time.

4.3. Traffic composition

We defined two types of vehicles (cars and trucks), which have different lengths (4 and 15 m, respectively). Traffic consists of 16.7% trucks, which is the truck percentage observed in the empirical data (Patire and Cassidy, 2011) that was used to calibrate the traffic model. We assume that cars can be controlled (i.e., equipped with one of the ACC systems) or non-controlled (i.e., human-driven). The longitudinal movement of controlled cars is regulated by their ACC controllers, whereas that of non-controlled cars is regulated by their drivers, which is modeled here using a car-following model (see Section 4.5). Furthermore, both controlled and non-controlled cars can change lanes, which we modeled using a lane change model (see Section 4.6).

Note that we defined three types of drivers for non-controlled cars (Car I, Car II and Car III). The car driver type is defined by the lane that cars are in when they enter the simulated network: cars that enter on the shoulder lane are assigned the type “Car I”, those that enter on the center lane are assigned the type “Car II”, and those that enter on the median lane are assigned the type “Car III”. Defining driver types in this manner was necessary to account for the differences in average driving behavior between lanes observed in empirical traffic data (Patire and Cassidy, 2011). Longitudinal and lateral driving behavior is modeled in the same way for the three types of non-controlled car drivers and for truck drivers, but the values of the model parameters are different (see Sections 4.5 and 4.6).

4.4. ACC controllers

The longitudinal movement of controlled cars along the road is automatically regulated by their ACC systems. We assume that trucks are not equipped with any type of ACC system. The formulation of the ACC controllers is described in Section 3 and the parameter values are presented in Table 1. The controller parameter values are assumed to be the same for all equipped vehicles. Note that, in this study, the controller parameter values were tuned manually. They could be tuned further (using an optimization method) to improve the performance of the ACC controllers, but this is left to future research.

4.5. Longitudinal driving behavior (non-controlled vehicles)

To describe the longitudinal driving behavior of the drivers of non-controlled vehicles (cars and trucks), we used a car-following model that determines the acceleration of vehicle i (a_i^{NC}) in every time step τ. A different counter than κ is used here because the time step length may be different than that of the ACC control time step. We assume that acceleration is constant over the whole duration of every time step τ. The time step length is denoted by $\Delta\tau$.

The car-following model determines the acceleration $a_i^{\mathrm{NC}}(\tau)$ based on a two-term function. The first term (f_i^{R}) describes regular car-following behavior, whereas the other one (f_i^{G}) accounts for the influence of the freeway’s vertical profile:

$$a_i^{\mathrm{NC}}(\tau) = f_i^{\mathrm{R}}(\tau) + f_i^{\mathrm{G}}(\tau) \tag{15}$$

Table 1
ACC controllers: parameter values.

B-ACC		TSA-ACC (additional)		CACC (additional)	
v_{d} (km/h)	100	v_{free} (km/h)	80	K_3 (m/s)	15
T_{d} (s)	1.2	v_{cong} (km/h)	60	r_{V2V} (m)	300
K_1 (s^{-1})	0.2	λ_{a} (km/h)	−10		
K_2 (m/s)	15	λ_{l} (km/h)	8		
$r_{\mathrm{B-ACC}}$ (m)	150	T_{r} (s)	4		
s_{s} (m)	3	T_{d}^{0} (s)	1.2		
$\mathrm{TTC}_{\mathrm{min}}$ (s)	2	$T_{\mathrm{d}}^{\mathrm{L}}$ (s)	0.8		
s_{min} (m)	8	$T_{\mathrm{d}}^{\mathrm{H}}$ (s)	1.6		
a_{min} ($\mathrm{m/s^2}$)	−8	T_{imp} (s)	6		
a_{max} ($\mathrm{m/s^2}$)	1.4				

The formulation of the first term is given by the IDM+ model (Schakel et al., 2012) (see Eqs. (16) and (17)), which is based on the Intelligent Driver Model (Treiber et al., 2000). The IDM+ assumes that, in unconstrained driving conditions, the acceleration of a vehicle depends mainly on its speed (v_i). Vehicles accelerate starting at the maximum acceleration α and reduce the acceleration rate as the speed approaches the desired speed v_0. The rate of reduction is given by δ, for which a value of 4 is generally used. Instead, in constrained driving conditions, drivers respond to the distance gap s_i, which is desired to be $s_0 + v_i \cdot T$ (where s_0 is the distance gap at standstill and T is the desired time gap). Additionally, a response to the approaching rate Δv_i is included. It is assumed that drivers aim to decelerate with rates lower than β, the maximum comfortable deceleration.

$$f_i^{\mathrm{R}}(\tau) = \alpha \cdot \min\left(1 - \left(\frac{v_i(\tau)}{v_0}\right)^{\delta}, 1 - \left(\frac{s_i^*(\tau)}{s_i(\tau)}\right)^2\right) \tag{16}$$

where:

$$s_i^*(\tau) = s_0 + v_i(\tau) \cdot T + \frac{v_i(\tau) \cdot \Delta v_i(\tau)}{2\sqrt{\alpha \cdot \beta}} \tag{17}$$

The second term in Eq. (15) (f_i^{G}) corresponds to the difference between the gradient at the location where vehicle i is at a given time step ($G_i(\tau)$) and the gradient compensated by the driver until that time step ($G_i^{\mathrm{c}}(\tau)$), multiplied by a sensitivity parameter (θ).

$$f_i^{\mathrm{G}}(t) = -\theta \cdot (G_i(\tau) - G_i^{\mathrm{c}}(\tau)) \tag{18}$$

The compensated gradient (G_i^{c}) is a variable that accounts for the fact that drivers show a limited ability to accelerate along sags. On the basis of findings reported by Yoshizawa et al. (2012), we assume that drivers compensate for positive changes in slope linearly over time (with a maximum gradient compensation rate defined by parameter c). Moreover, the model assumes that drivers can immediately compensate for negative changes in gradient. Therefore:

- If $G_i(\tau) \leqslant G_i^{\mathrm{c}}(\tau - 1) + c \cdot \Delta\tau$:

$$G_i^{\mathrm{c}}(\tau) = G_i(\tau) \tag{19}$$

- If $G_i(\tau) > G_i^{\mathrm{c}}(\tau - 1) + c \cdot \Delta\tau$:

$$G_i^{\mathrm{c}}(\tau) = G_i^{\mathrm{c}}(\tau - 1) + c \cdot \Delta\tau \tag{20}$$

This implies that, if the driver's maximum gradient compensation rate (c) is lower than the rate at which the freeway slope increases over time, then $G_i^{\mathrm{c}} < G_i$ for a certain period of time. During this period, G_i^{c} increases linearly over time but f_i^{G} is negative (see Eq. (18)), which limits acceleration (see Eq. (15), and Fig. 1 in Goñi-Ros et al. (2015)). This limitation in vehicle acceleration appears to be the main cause of the local changes in longitudinal driving behavior that reduce the freeway capacity at sags (Yoshizawa et al., 2012; Goñi-Ros et al., 2014a). Note that, in the first time step ($\tau = 0$), the compensated gradient is set to be equal to the value of the gradient at the initial position (i.e., $G_i^{\mathrm{c}}(0) = G_i(0)$).

For more details on the properties of the car-following model and a demonstration of its face-validity, we refer to Goñi-Ros et al. (2015, 2016a). The parameter values used in this research are shown in Table 2. Note that parameters v_0, α, β, T and c were set to be stochastic, so their values differ per vehicle. The stochastic parameter values are normally distributed with the means being the values shown in Table 2 (see also Appendix). The parameters in Tables 2 and 4 (Appendix) have been manually calibrated to match the macroscopic traffic patterns observed at the Yamato sag of the Tomei Expressway (Japan) (Patire and Cassidy, 2011).

4.6. Lateral driving behavior

To describe lateral driving behavior, we use the Lane Change Model with Relaxation and Synchronization (LMRS) by Schakel et al. (2012) integrated with the car-following model described in Section 4.5. Note that both controlled and non-controlled vehicles can change lanes. During a lane change it is assumed that the driver follows two leading vehicles. When the lane change ends, the driver enables the system when equipped. It is furthermore assumed that drivers of equipped vehicles do not alter their lane change decisions. Although this might not be completely realistic, it is a conservative assumption as ACC tends to lower the number of lane changes performed (Schakel et al., 2017). Note that lane changes could reduce the efficiency of the proposed systems (i.e. reducing the number of lane changes could potentially improve the results). Therefore, we use the same lane change model (integrated with the car-following model) for both types of vehicles.

The main principle of the LMRS is that a set of lane change incentives results in a single lane change desire (d), and lane-changing behavior depends on this level of desire. There are four regimes determined by the level of desire (see Eq. (21)). In the first regime, no lane change is initiated. In the second regime, lane changes are performed without any preparation (if they are possible). If $d \geqslant d_{\mathrm{sync}}$, the driver starts to synchronize with the leader in the target lane in order to prepare for a lane change; and if $d \geqslant d_{\mathrm{coop}}$, the follower in the target lane starts to create a gap for the lane changer (these phenomena have been observed, for example, in Yeo et al. (2008)).

Table 2
Driving behavior models: parameter values.

	Driver type			
	Car I	Car II	Car III	Truck
		Car-following model		
$\bar{v}_0$ (km/h)	85	95	110	85
$\bar{\alpha}$ (m/s^2)	1.4	1.4	1.4	0.7
$\bar{\beta}$ (m/s^2)	2.1	2.1	2.1	1.5
δ (–)	4	4	4	4
s_0 (m)	3	3	3	4
$\bar{T}$ (s)	1.3	1.3	1.3	2.0
θ (m/s^2)	22	22	22	22
$\bar{c}$ (s^{-1})	0.0004	0.0004	0.0004	0.0004
		Lane change model		
d_{free} (–)	0.365	0.365	0.365	0.365
d_{sync} (–)	0.577	0.577	0.577	0.577
d_{coop} (–)	0.788	0.788	0.788	0.788
v_{gain} (km/h)	60	50	40	60
v_{crit} (km/h)	60	60	60	60
x_0 (m)	200	200	200	200
$\bar{T}_{\text{min}}$ (s)	0.56	0.56	0.56	0.56
T_{rel} (s)	25	25	25	25

$$0 < d_{\text{free}} < d_{\text{sync}} < d_{\text{coop}} < 1 \tag{21}$$

Moreover, as d increases, the acceptable time gap (evaluated with the car following model) becomes shorter than the default value T (but never shorter than the lower bound T_{min}). This is known as the relaxation phenomenon (Laval and Leclercq, 2008). After the lane change is executed, the acceptable time gap goes back to the default value (over some time). Since speed is adjusted to the target lane and shorter time gaps are temporarily accepted, the LMRS allows realistic lane changes.

For more details on the properties of the lane change model, a full description of its parameters, and the model calibration results, we refer to Schakel et al. (2012). The parameter values for non-controlled vehicles are shown in Table 2. These are the same values reported in Schakel et al. (2012) except for the values of parameters x_0 and v_{gain}, which we have adjusted (slightly) to (better) match the macroscopic patterns observed at the Yamato sag of the Tomei Expressway (Japan) (Patire and Cassidy, 2011). The parameter values for ACC-equipped cars are the same as for non-controlled vehicles except for v_{gain}, which is equal to 70 km/h. Note that T_{min} is a stochastic parameter. Its values in the vehicle population are normally distributed. Details of the used stochastic distributions are presented in the Appendix.

4.7. Vehicle dynamics

The speed and position of a controlled car are updated as follows:

$$v_i(\kappa + 1) = v_i(\kappa) + a_i^{\text{C}}(\kappa)\cdot\Delta\kappa \tag{22}$$

$$x_i\left(\kappa + 1\right) = x_i(\kappa) + v_i(\kappa)\cdot\Delta\kappa + \frac{a_i^{\text{C}}(\kappa)\cdot\Delta\kappa^2}{2} \tag{23}$$

where a_i^{C} corresponds to $a_i^{\text{B-ACC}}$, $a_i^{\text{TSA-ACC}}$ or $a_i^{\text{C-ACC}}$ depending on the system the car is equipped with.

The speed and position of a non-controlled vehicle are updated using formulas equivalent to Eqs. (22) and (23) where κ, a_i^{C} and $\Delta\kappa$ are subsituted by τ, a_i^{NC} and $\Delta\tau$, respectively. Accelerations a_i^{C} and a_i^{NC} are assumed to be instantly realizable. When the position and speed of a vehicle in time step $\kappa + 1$ (or $\tau + 1$) are known, its acceleration can be recalculated for that time step, and so on. In principle, a time step ($\Delta\kappa = \Delta\tau$) would give the simulation a solution which is closer to the idealised model. A long update time would give the risk of vehicles not updating the speed fast enough, which might result in collisions. In this study, we assume that $\Delta\kappa = \Delta\tau = 0.5$ s, which is (together with 0.1 s) one of the most frequently chosen values in this type of simulation studies. With the choice of 0.5 s, trajectories were realistic enough and we did not encounter any problems with collisions, so there was no need to shorten it further.

Lane changes are not performed immediately. Right after the decision to change lanes has been made and a gap has been accepted, a ghost vehicle is created in the target lane. During 3 s, vehicles in the target lane move as if the lane-changing vehicle was already there (i.e., they react to the movement of the ghost vehicle). After these 3 s, the lane-changing vehicle leaves the origin lane and takes the place of the ghost vehicle in the target lane.

4.8. Scenarios

Various scenarios were defined by setting different values for the percentage of cars equipped with ACC systems (0%, 10%, 20%, 30%, 50%, 75% and 100%), and the type of ACC system that cars are equipped with (B-ACC, TSA-ACC and C-ACC). A scenario was defined for all possible combinations, giving 19 scenarios (i.e., 1 (0% penetration rate) + 3 (types of ACC systems) × 6 (non-zero penetration rates) = 19). 20 simulations runs were performed for each scenario. Recall that we assume that trucks are not equipped with any ACC system.

4.9. Effectiveness indicators

The effectiveness of the ACC controllers was evaluated by comparing the average travel time and average vehicle delay between locations $x = 0.6$ km (4.1 km upstream of the sag) and $x = 6.4$ km (1.1 km downstream of the sag) in the different scenarios. We calculated the means of the average travel time ($\overline{\text{ATT}}$) and the average vehicle delay ($\overline{\text{AVD}}$) in the 20 simulation runs of each scenario, as well as the first and third quartiles. Lower values of $\overline{\text{ATT}}$ and $\overline{\text{AVD}}$ indicate less severe traffic congestion.

The average travel time corresponding to simulation run ρ of a certain scenario is calculated as follows:

$$\text{ATT}_\rho = \frac{\sum_{m=m_{1,\rho}}^{m_{\text{F},\rho}} \text{TT}_{m,\rho}}{N_\rho} \tag{24}$$

where $m_{1,\rho}$ and $m_{\text{F},\rho}$ are the values of the first and last elements of set M_ρ, which contains the counters i of all vehicles (cars and trucks) that reach location $x = 6.4$ km before the end of the simulation period in run ρ in ascending order ($M_\rho = \{m_{1,\rho}, m_{2,\rho}, \ldots, m_{\text{F},\rho}\}$); N_ρ is the cardinality of set M_ρ; and $\text{TT}_{m,\rho}$ is the travel time of vehicle m in run ρ.

The average vehicle delay corresponding to simulation run ρ of a given scenario is calculated as follows:

$$\text{AVD}_\rho = \text{ATT}_\rho - \text{ATT}^{\text{CG}} \tag{25}$$

where ATT^{CG} is the average travel time in a reference scenario where the gradient of the simulated freeway stretch is assumed to be constant (i.e., there is no sag) and no vehicle is equipped with any ACC system (i.e., the penetration rate is 0%).

ATT^{CG} is calculated analytically under the assumption that the movement of all vehicles is completely unhindered by other traffic (or the sag), thus they travel at the desired speed (v_0) of their drivers. Here we assume that the desired speeds are deterministic and equal to the mean desired speeds shown in Table 2, which depend on the driver type. The distribution of cars per driver type was calculated using the lane flow distribution model Hong and Oguchi (2008) assuming a constant demand equal to the highest demand given as input (5200 veh/h) and a 16.7% truck percentage. ATT^{CG} constitutes a theoretical lower bound on average travel time for a given traffic composition, which can be used to evaluate the performance of the controllers. Note that, with moderate/high traffic flows (also in free flow conditions), this theoretical lower bound is usually not achieved: vehicles always experience some delay since they are bound by the speed of their preceding vehicle. In our case, ATT^{CG} equals 3.56 min. This value is used to calculate the AVD_ρ of all simulation runs ρ of all scenarios (using Eq. (25)) and, therefore, to compare the performance of all ACC controllers assuming different penetration rates.

Speed-contour plots are used to assess changes in traffic flow dynamics resulting from the different ACC systems, and were compared with the no-control scenario and with each other. The plots are based on trajectory data aggregated over space and time with a 10 m × 5 s granularity.

The controllers do not only influence the queue outflow, but since spacing changes, also the queue length changes, which can have important consequences if there are on- or off-ramps (Knoop et al., 2008). Maximum queue lengths are calculated in order to assess possible spillback effects, e.g. for cases with nearby upstream off-ramps. The maximum queue length is defined as the longest consecutive string of cells (10 m in length) in the speed-contour plots at a specific time (cells of 5 s) but on any lane, with speeds below 60 km/h.

5. Results

This section presents the results of the ACC controller evaluation. Controller performance is analyzed by comparing the values of $\overline{\text{ATT}}$ and $\overline{\text{AVD}}$ in various scenarios, and explaining what effects the ACC controllers have on traffic flow that lead to the differences in $\overline{\text{ATT}}$ and $\overline{\text{AVD}}$. Note that, for all scenarios, the average travel time (ATT) varies between different simulation runs (see Fig. 3). This is due to model stochasticity (see Sections 4.5, 4.6 and Appendix). However, that variation is small in all scenarios. This indicates that the performance of the ACC controllers is quite robust and justifies using the mean ATT and AVD (i.e., $\overline{\text{ATT}}$ and $\overline{\text{AVD}}$) as indicators of controller performance.

As shown in Fig. 3, $\overline{\text{ATT}}$ decreases if the percentage of cars equipped with B-ACC increases between 0 and 75% (in the scenario with 100% penetration rate, $\overline{\text{ATT}}$ has the same value as in the scenario with 75% penetration rate). Therefore, $\overline{\text{AVD}}$ also decreases with increasing penetration rate, reaching a value 59% lower than in the no-control scenario in the scenarios with 75 and 100% penetration rate (see Table 3). The reason is that equipping cars with the B-ACC system increases the capacity of the sag (both in free-flow and congested traffic conditions). As a result, traffic breaks down at higher flow rates and the outflow from congestion is higher, which leads to decreased $\overline{\text{ATT}}$. The higher the penetration rate, the higher the sag capacity, and the lower the $\overline{\text{ATT}}$ (Fig. 3). With a penetration rate of 75% or higher, the sag capacity becomes high enough to accomodate the traffic demand; thus, traffic no longer

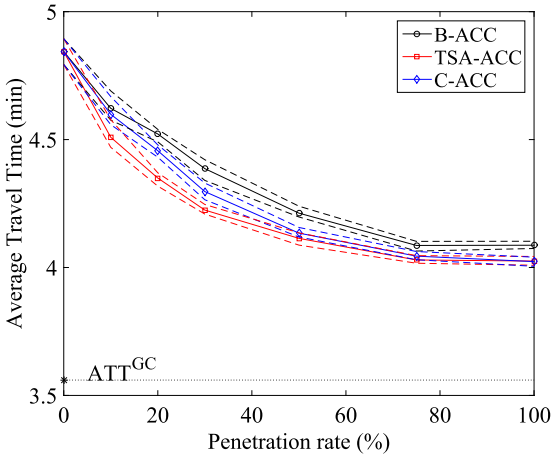

Fig. 3. Average Travel Time (ATT): mean, first and third quartiles of 20 simulation runs of every scenario. The means are shown by solid lines with markers, whereas the quartiles are shown by dashed lines. The Average Travel Time in the reference scenario (ATT^{CG}) is shown by an asterisk marker.

Table 3
Mean average vehicle delay ($\overline{AVD}$) in all scenarios.

Pen. Rate (%)	B-ACC		TSA-ACC		C-ACC	
	$\overline{AVD}$ (min)	Δ $\overline{AVD}$ (%)	$\overline{AVD}$ (min)	Δ $\overline{AVD}$ (%)	$\overline{AVD}$ (min)	Δ $\overline{AVD}$ (%)
0	1.28	0	1.28	0	1.28	0
10	1.06	−17	0.95	−26	1.04	−19
20	0.96	−25	0.79	−38	0.90	−30
30	0.83	−35	0.66	−48	0.74	−42
50	0.65	−49	0.55	−57	0.57	−55
75	0.53	−59	0.47	−63	0.48	−63
100	0.53	−59	0.47	−63	0.46	−64

becomes fully congested at the bottleneck (although traffic slows down at the sag and some short-lived episodes of congestion occur), and $\overline{ATT}$ does not decrease further (see Fig. 3).

As in the case of B-ACC, equipping cars with the TSA-ACC system also results in decreased $\overline{ATT}$. Fig. 3 shows that $\overline{ATT}$ decreases if the percentage of cars equipped with TSA-ACC increases between 0 and 75% (again, $\overline{ATT}$ does not decrease further if the penetration rate goes above 75%). Furthermore, note that TSA-ACC reduces $\overline{ATT}$ more than B-ACC in all scenarios (Fig. 3). The main reason is that equipping cars with the TSA-ACC system instead of the B-ACC system leads to higher queue discharge rates. The greatest differences in effectiveness between the TSA-ACC and B-ACC controllers are observed in the scenarios with 10–50% penetration rates (TSA-ACC reduces $\overline{AVD}$ by 8–13% more in comparison to the no-control scenario, as shown in Table 3). The value of $\overline{ATT}$ in the scenario with 50% penetration rate is very close to the value of $\overline{ATT}$ in the scenario with a penetration rate of B-ACC-equipped cars equal to 75% (see Fig. 3), in which traffic does not become fully congested at the bottleneck. This suggests that equipping 50% of the cars with the TSA-ACC system removes congestion from the bottleneck almost entirely. With penetration rates of TSA-ACC higher than 50%, traffic no longer becomes fully congested at the bottleneck (thus $\overline{ATT}$ is the same in these scenarios). Because of this, the TSA-ACC controller does not perform much differently than the B-ACC controller. Note, however, that the TSA-ACC controller performs slightly better (see Table 3). The main reason is that the short-lived episodes of congestion that occur at the sag in the scenarios with 75 and 100% penetration rate are shorter if controlled vehicles are equipped with TSA-ACC instead of B-ACC.

Equipping cars with the C-ACC system also reduces the $\overline{ATT}$ in comparison with the no-control scenario. As shown in Fig. 3, $\overline{ATT}$ decreases if the percentage of cars equipped with C-ACC increases between 0 and 75%. Again, in the scenario with 100% penetration rate, $\overline{ATT}$ has almost the same value as in the scenario with 75% penetration rate. Also, note that C-ACC is able to reduce $\overline{ATT}$ more than B-ACC in all scenarios (as with TSA-ACC, the main reason is a comparative increase in queue discharge rates). The greatest differences in effectiveness between B-ACC and C-ACC are observed with penetration rates of 30 and 50% (6–7% greater reduction in $\overline{AVD}$ in comparison with the no-control scenario, as shown in Table 3). The main reason is that the C-ACC controller only behaves differently than the B-ACC controller if there are cars equipped with C-ACC within a certain distance, which becomes more likely if the penetration rate increases. With very high penetration rates of B-ACC or C-ACC (75 and 100%) traffic does not become fully congested at the bottleneck, so the additional benefits of C-ACC compared to B-ACC become less significant. Nevertheless, with these penetration rates, C-ACC still outperforms B-ACC (see Table 3), because the short-lived episodes of congestion that occur at the sag become shorter. Moreover, note that the TSA-ACC controller reduces $\overline{AVD}$ more than the C-ACC controller (5–7% greater reduction in $\overline{AVD}$ in comparison with the no-control scenario) with low/moderate penetration rates (10–30%), whereas the effectiveness of these

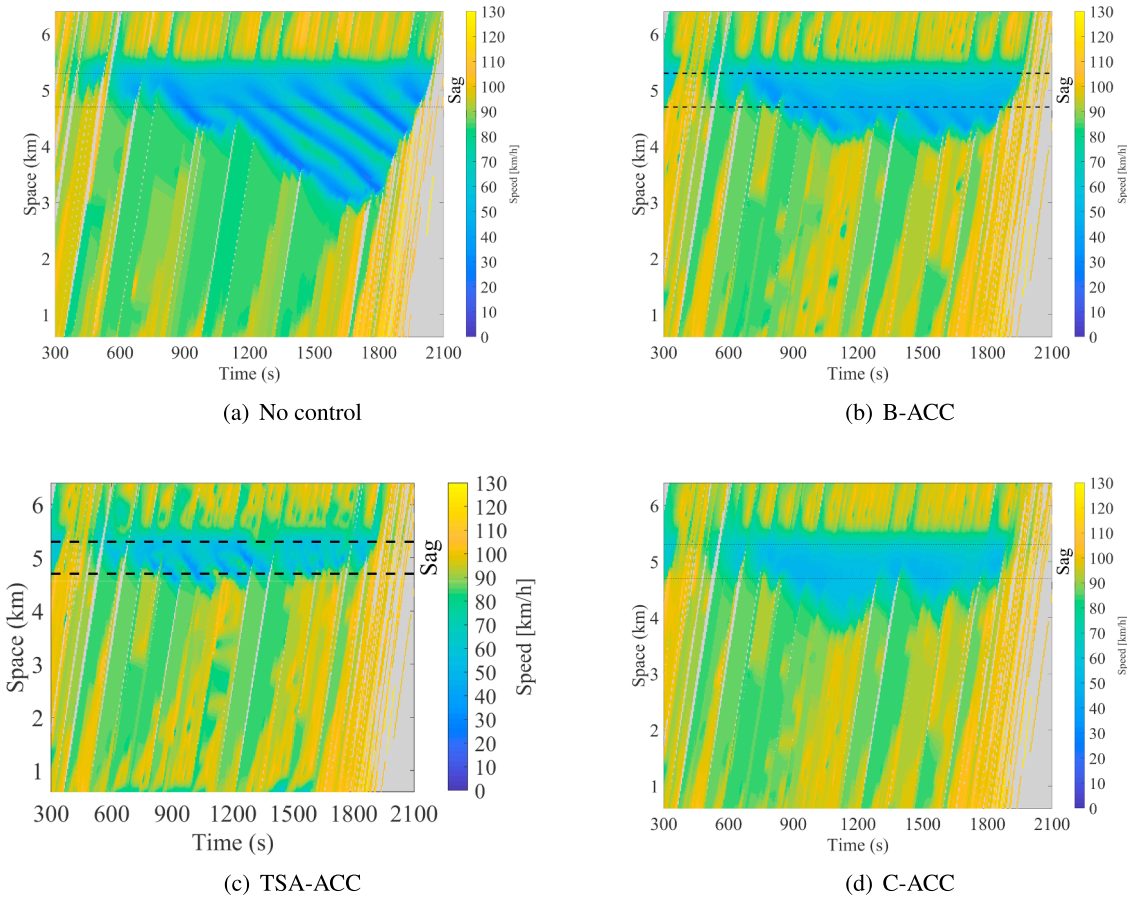

Fig. 4. Speed-contour plots on the median lane in the first run. For the scenarios with ACC systems (b, c and d) the penetration rate is 30%.

two controllers is similar with high penetration rates (50–100%), as shown in Table 3.

The speed-contour plots in Fig. 4 show interesting points concerning traffic stability under the different controllers. TSA-ACC creates pronounced and short moving jams. B-ACC creates moving jams from a smoother bottleneck, while C-ACC creates near-homogeneous congestion with no discernible moving jams. From the simulated trajectories, we can observe that disturbances in the B-ACC platoon are amplified while those in the C-ACC platoon are attenuated. From these observations, it seems the B-ACC platoon is string unstable while the C-ACC platoon is string stable. We cannot say whether the TSA-ACC is string stable or not because it involves switching of the desired time gap at different operational modes. We acknowledge that there are more elegant ways to analyse the string stability properties of the ACC controllers, e.g. Treiber and Kesting (2011).

Fig. 4 shows the traffic flow dynamics on the median lane for each ACC system at 30% penetration rate, and for the no-control scenario. Besides the ACC controllers clearly reducing the level of congestion, the differences in traffic flow dynamics are remarkable. B-ACC results in smooth dynamics in the sag vertical curve (between 4.7 km and 5.3 km). The resulting moving jams are less pronounced and shorter. The active approach of the TSA-ACC controller presents very different dynamics, with short and quickly resolved moving jams. The moving jams are pronounced as the outflow is increased. During high demand the moving jams keep appearing as the system can only respond once congestion arises. Finally, C-ACC results in near-homogeneous congestion in which no moving jams are discernible. The control law is capable of stabilizing congested flow while increasing the queue outflow. These findings also hold for the other lanes, but to a lesser extent (most likely due to the presence of trucks). It is also found that for 75% and 100% penetration rate, where the systems are not able to improve efficiency further, the remaining congestion starts and is most severe on the shoulder lane. This is due to trucks not being equipped, which also explains why no further efficiency gains are achieved.

Fig. 5 shows the maximum queue length distribution. The main message is that a pattern is visible where the queue length is reduced due to increased efficiency, with the most efficient ACC controller generally resulting in the shortest queues. This is typically at around 75% penetration rate. Still, for some penetration ranges the maximum queue length increases with the penetration rate. This is visible for B-ACC (10% and 20%), C-ACC (10%) and all systems at 100% penetration rate. At low penetration rates B-ACC and C-ACC do not increase efficiency sufficiently to also decrease queue length. At 100% all systems are unable to increase efficiency further, and hence queue lengths increase relative to 75% penetration rate. However, in this case, the maximum queue is still lower than in the no-control scenario.

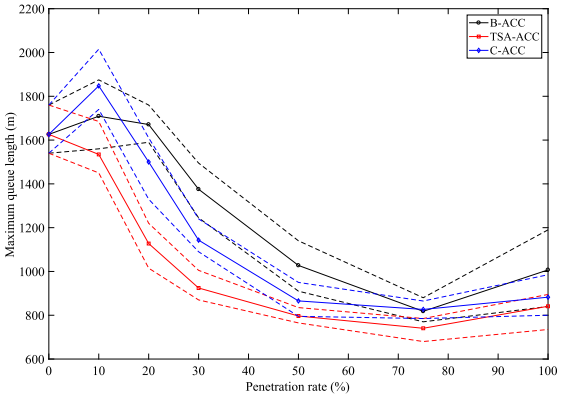

Fig. 5. Maximum queue length distribution. Dashed lines indicated the first and third quartiles. Continuous lines indicated the average over 20 simulation runs.

It should be remarked that no collisions between vehicles occurred in the simulations. Furthermore, the ACC controllers did not show locally unstable behavior (which can cause traffic-disruptive and potentially unsafe situations) in any simulation run.

6. Conclusions

Previous research suggests that traffic management measures based on the use of advanced ACC systems can potentially reduce congestion on freeways. The main goal of this article was to evaluate the effectiveness of a basic ACC system (B-ACC) and two advanced ACC systems (Traffic State-Adaptive ACC, TSA-ACC, and Cooperative ACC, C-ACC) in mitigating congestion at freeway sags. The performance of these ACC systems was evaluated by means of microscopic traffic simulations with different penetration rates. The simulations assumed no delays in processing or communication for the ACC systems.

The results show that equipping vehicles with the basic ACC system can reduce congestion at sags under high-demand conditions. Congestion decreases with increasing penetration rate and, with high penetration rates, only mild congestion starting on the shoulder lanes remains due to trucks not being equipped. The reason is that the acceleration behavior of equipped vehicles is not affected by the freeway gradient. Therefore, the presence of these vehicle increases the sag capacity (both in free flow and congestion), even if the system's desired time gap is similar to that of human drivers. These findings are in line with those of previous studies (Ozaki, 2003; Goñi-Ros et al., 2016b).

Importantly, furthermore, the results indicate that equipping vehicles with the Traffic State-Adaptive ACC (TSA-ACC) or Cooperative ACC (C-ACC) systems reduces congestion even more than the basic ACC system. As a result, these systems can prevent congestion at lower penetration rates. This is due to the additional features of the TSA-ACC and C-ACC controllers, which cause a comparative increase in the queue discharge capacity of the sag. Note, however, that the C-ACC system needs penetration rates above 20% to significantly outperform the basic ACC system. Below this percentage, the level of connectivity between equipped vehicles is too low, so the C-ACC system operates similarly to the basic ACC system. In general, the TSA-ACC system is more effective than the C-ACC system. However, it should be noted that the C-ACC controller proposed here does not use a shorter desired time gap than the basic ACC controller. With such control settings, the C-ACC system may outperform the TSA-ACC system.

For cases with nearby upstream off-ramps, the resulting queue length is of importance. Generally, the gain in efficiency reduces the queue lengths, but at low penetration rates both B-ACC and C-ACC tend to increase queue length by a few 100 meters in our case. Optimization on this issue will likely reduce the queue lengths, but it remains to be investigated how this is best balanced with efficiency.

The findings reported in this article support the development of traffic management measures for sags based on the use of advanced ACC systems. Further research should investigate the effectiveness of the TSA-ACC and C-ACC systems in real freeways. Field tests would also help to improve the design of these systems (e.g., controller parameter tuning, additional features) and improve their effectiveness in reducing congestion at sags. Traffic flow dynamics are changed in different ways by the various systems. B-ACC and C-ACC smoothen disturbances, while TSA-ACC results in short and pronounced moving jams. There is no direct correlation between such stability and efficiency, as TSA-ACC is the most efficient. Local and string stability analyses of the proposed ACC controllers are worth investigation in the next steps. In fact, the ACC-controller parameters can be optimized to improve their string stability performance using string stability analysis (Jin and Orosz, 2014) and controller synthesis techniques (Ploeg et al., 2014a). Finally, there is room to develop other types of advanced ACC systems able to reduce congestion at sags. A promising direction seems to be integrating inflow control measures with ACC systems (Goñi-Ros et al., 2016b; Nezafat et al., 2018).

Acknowledgments

The research reported in this paper was funded by Toyota Motor Europe. The authors thank the anonymous reviewers for their comments, which have led to considerable improvements in the paper.

Table 4
Standard deviations of distributions $\mathcal{N}_1^{\phi}(\mu, \sigma_1^{\phi})$, $\mathcal{N}_2^{\phi}(\mu, \sigma_2^{\phi})$, $\mathcal{N}_3^{\phi}(\mu, \sigma_3^{\phi})$ and $\mathcal{N}_4^{\phi}(\mu, \sigma_4^{\phi})$.

Parameter	Driver type (ϕ)			
	Car I	Car II	Car III	Truck
σ_1^{ϕ}	0.01	0.05	0.1	0.01
σ_2^{ϕ}	0.01	0.01	0.05	0.01
σ_3^{ϕ}	0.01	0.01	0.01	0.01
σ_4^{ϕ}	0.05	0.05	0.05	0.01

Appendix A. Method used to define the values of the stochastic parameters of the driving behavior models

As mentioned in Section 4, the following parameters of the car-following and lane change models were set to be stochastic: desired speed (v_0); maximum acceleration (α); maximum comfortable deceleration (β); desired time gap (T); maximum gradient compensation rate (c); lower bound of the acceptable time gap during lane changes ($T_{\min}$). This is done to account for heterogeneity in driving behavior, which is an important characteristic of freeway traffic flow (Patire and Cassidy, 2011; Ossen and Hoogendoorn, 2011).

In our simulation experiments, each vehicle is assigned a value for every model parameter when it is generated and enters the simulated network. The values of the deterministic parameters are the same for all vehicles. On the other hand, the values of the stochastic parameters differ among vehicles, and they are generated as follows. Firstly, before starting the simulation, we create four Normal distributions per driver type (i.e., sixteen distributions in total), all of them with unit mean ($\mu = 1$). These distributions can be denoted by $\mathcal{N}_1^{\phi}(\mu, \sigma_1^{\phi})$, $\mathcal{N}_2^{\phi}(\mu, \sigma_2^{\phi})$, $\mathcal{N}_3^{\phi}(\mu, \sigma_3^{\phi})$ and $\mathcal{N}_4^{\phi}(\mu, \sigma_4^{\phi})$, where the symbol ϕ indicates the driver type (ϕ can be any of the strings contained in set Φ = {CarI, CarII, CarIII, Truck}, which correspond to the driver types defined in Section 4.3). The standard deviations of these Normal distributions are shown in Table 4. Secondly, when a given vehicle is generated, a value is randomly drawn from each of the four Normal distributions associated to the driver type assigned to that vehicle (within the range $[\mu - 3\sigma, \mu + 3\sigma]$). Let us denote the drawn values by ω_1, ω_2 ω_3 and ω_4. Then, the values of the stochastic parameters are determined as follows: $v_0 = \bar{v}_0 \cdot \omega_1$; $\alpha = \bar{\alpha} \cdot \omega_2$; $\beta = \bar{\beta} \cdot \omega_2$; $T = \overline{T} \cdot \omega_4$; $c = \bar{c}/\omega_3$; and $T_{\min} = \overline{T}_{\min}/\omega_1$. Note that the values of some stochastic parameters are correlated. For instance, drivers with higher desired speeds (v_0) are considered more aggressive and are made to accept shorter time gaps when changing lanes ($T_{\min}$).

References

Brilon, W., Bressler, A., 2004. Traffic flow on freeway upgrades. Transport. Res. Rec.: J. Transport. Res. Board 1883, 112–121.

Carlson, R., Papamichail, I., Papageorgiou, M., 2011. Local feedback-based mainstream traffic flow control on motorways using variable speed limits. IEEE Trans. Intell. Transport. Syst. 12 (4), 1261–1276.

Furuichi, T., Yamamoto, S., Kotani, M., Iwasaki, M., 2003. Characteristics of spatial speed change at motorway sag sections and capacity bottlenecks. In: 82nd Annual Meeting of the Transportation Research Board.

Goñi-Ros, B., Knoop, V., van Arem, B., Hoogendoorn, S.P., 2014a. Empirical analysis of the causes of stop-and-go waves at sags. IET Intell. Transport Syst. 8 (5), 499–506.

Goñi-Ros, B., Knoop, V., van Arem, B., Hoogendoorn, S.P., 2014b. Mainstream traffic flow control at sags. Transport. Res. Rec.: J. Transport. Res. Board 2470, 57–64.

Goñi-Ros, B., Knoop, V.L., Schakel, W.J., van Arem, B., Hoogendoorn, S.P., 2015. A model of car-following behavior at sags. In: Traffic and Granular Flow'13. Springer, pp. 385–393.

Goñi-Ros, B., Knoop, V.L., Shiomi, Y., Takahashi, T., van Arem, B., Hoogendoorn, S.P., 2016a. Modeling traffic at sags. Int. J. Intell. Transport. Syst. Res. 14 (1), 64–74.

Goñi-Ros, B., Knoop, V.L., Takahashi, T., Sakata, I., Van Arem, B., Hoogendoorn, S.P., 2016b. Optimization of traffic flow at freeway sags by controlling the acceleration of vehicles equipped with in-car systems. Transport. Res. Part C: Emerg. Technol. 71, 1–18.

Hall, F.L., Agyemang-Duah, K., 1991. Freeway capacity drop and the definition of capacity. Transport. Res. Rec.: J. Transport. Res. Board 1320, 91–98.

Hatakenaka, H., Hirasawa, T., Yamada, K., Yamada, H., Katayama, Y., Maeda, M., 2006. Development of AHS for traffic congestion in sag sections. In: 13th ITS World Congress.

Hong, S., Oguchi, T., 2008. Lane use and speed-flow relationship on basic segments of multilane motorways in Japan. In: 87th Annual Meeting of the Transportation Research Board.

Ioannou, P., Wang, Y., Chang, H., 2007. Integrated roadway/adaptive cruise control system: safety, performance, environmental and near term deployment considerations. California PATH Program, Institute of Transportation Studies, University of California at Berkeley.

Jin, I.G., Orosz, G., 2014. Dynamics of connected vehicle systems with delayed acceleration feedback. Transport. Res. Part C: Emerg. Technol. 46, 46–64.

Jin, I.G., Orosz, G., 2018. Connected cruise control among human-driven vehicles: experiment-based parameter estimation and optimal control design. Transport. Res. Part C: Emerg. Technol. 95, 445–459.

Jin, W.-L., 2018. Kinematic wave models of sag and tunnel bottlenecks. Transport. Res. Part B: Methodol. 107, 41–56.

Kesting, A., Treiber, M., Schnhof, M., Helbing, D., 2008. Adaptive cruise control design for active congestion avoidance. Transport. Res. Part C: Emerg. Technol. 16 (6), 668–683.

Knoop, V., Van Zuylen, H., Hoogendoorn, S., 2008. The influence of spillback modelling when assessing consequences of blockings in a road network. EJTIR 8 (4).

Koshi, M., 2003. An Interpretation of a Traffic Engineer on Vehicular Traffic Flow. Springer, Berlin, pp. 199–210 Chapter 18.

Koshi, M., Kuwahara, M., Akahane, H., 1992. Capacity of sags and tunnels on japanese motorways. ITE J. 62 (5), 17–22.

Laval, J.A., 2009. Effects of geometric design on freeway capacity: impacts of truck lane restrictions. Transport. Res. Part B: Methodol. 43 (6), 720–728.

Laval, J.A., Leclercq, L., 2008. Microscopic modeling of the relaxation phenomenon using a macroscopic lane-changing model. Transport. Res. Part B: Methodol. 42 (6), 511–522.

Liu, H., Kan, X.D., Shladover, S.E., Lu, X.-Y., Ferlis, R.E., 2018. Modeling impacts of cooperative adaptive cruise control on mixed traffic flow in multi-lane freeway

facilities. Transport. Res. Part C: Emerg. Technol. 95, 261–279.
Moon, S., Moon, I., Yi, K., 2009. Design, tuning and evaluation of a full-range adaptive cruise control system with collision avoidance. Control Eng. Pract. 17 (4), 442–455.
Nezafat, R.V., Beheshtitabar, E., Cetin, M., Williams, E., List, G.F., 2018. Modeling and evaluating traffic flow at sag curves when imposing variable speed limits on connected vehicles. Transport. Res. Rec. 2672 (20), 193–202.
Okamura, H., Watanabe, S., Watanabe, T., 2000. An empirical study on the capacity of bottlenecks on the basic suburban expressway sections in japan. In: Proceedings of the 4th International Symposium on Highway Capacity.
Ossen, S., Hoogendoorn, S.P., 2011. Heterogeneity in car-following behavior: theory and empirics. Transport. Res. Part C: Emerg. Technol. 19 (2), 182–195.
Ozaki, H., 2003. Modeling of Vehicular Behavior from Road Traffic Engineering Perspectives. Springer, Berlin pp. 281–292.
Papacharalampous, A., Wang, M., Knoop, V., Goñi-Ros, B., Takahashi, T., Sakata, I., van Arem, B., Hoogendoorn, S., 2015. Mitigating congestion at sags with adaptive cruise control systems. In: 18th IEEE International Conference on Intelligent Transportation Systems.
Papageorgiou, M., Diakaki, C., Dinopoulou, V., Kotsialos, A., Wang, Y., 2003. Review of road traffic control strategies. In: Proceedings of the IEEE, vol. 91, pp. 2043–2067.
Patire, A.D., Cassidy, M.J., 2011. Lane changing patterns of bane and benefit: observations of an uphill expressway. Transport. Res. Part B: Methodol. 45 (4), 656–666.
Ploeg, J., Shukla, D.P., van de Wouw, N., Nijmeijer, H., 2014a. Controller synthesis for string stability of vehicle platoons. IEEE Trans. Intell. Transport. Syst. 15 (2), 854–865.
Ploeg, J., Van De Wouw, N., Nijmeijer, H., 2014b. Lp string stability of cascaded systems: application to vehicle platooning. IEEE Trans. Control Syst. Technol. 22 (2), 786–793.
Roncoli, C., Papamichail, I., Papageorgiou, M., 2016. Hierarchical model predictive control for multi-lane motorways in presence of vehicle automation and communication systems. Transport. Res. Part C: Emerg. Technol. 62, 117–132.
Sato, H., Xing, J., Tanaka, S., Watauchi, T., 2009. An automatic traffic congestion mitigation system by providing real time information on head of queue. In: 16th ITS World Congress.
Scarinci, R., Heydecker, B., Hegyi, A., 2015. Analysis of traffic performance of a merging assistant strategy using cooperative vehicles. IEEE Trans. Intell. Transport. Syst. 16 (4), 2094–2103.
Schakel, W., Knoop, V., Van Arem, B., 2012. Integrated lane change model with relaxation and synchronization. Transport. Res. Rec.: J. Transport. Res. Board 2316, 47–57.
Schakel, W.J., Gorter, C.M., deWinter, J.C., van Arem, B., 2017. Driving characteristics and adaptive cruise control? A naturalistic driving study. IEEE Intell. Transport. Syst. Mag. 9 (2), 17–24.
Schakel, W.J., Van Arem, B., Netten, B.D., 2010. Effects of cooperative adaptive cruise control on traffic flow stability. In: 2010 13th International IEEE Conference on Intelligent Transportation Systems (ITSC). IEEE, pp. 759–764.
Shladover, S., Su, D., Lu, X.-Y., 2012. Impacts of cooperative adaptive cruise control on freeway traffic flow. Transport. Res. Rec.: J. Transport. Res. Board (2324), 63–70.
Spiliopoulou, A., Manolis, D., Vandorou, F., Papageorgiou, M., 2018. Adaptive cruise control operation for improved motorway traffic flow. Transport. Res. Record 2672 (22), 24–35 0361198118796020.
Spiliopoulou, A., Perraki, G., Papageorgiou, M., Roncoli, C., 2017. Exploitation of ACC systems towards improved traffic flow efficiency on motorways. In: 2017 5th IEEE International Conference on Models and Technologies for Intelligent Transportation Systems (MT-ITS). IEEE, pp. 37–43.
Sun, J., Li, T., Yu, M., Zhang, H.M., 2018. Exploring the congestion pattern at long-queued tunnel sag and increasing the efficiency by control. IEEE Trans. Intell. Transport. Syst. 19 (12), 3765–3774.
Treiber, M., Hennecke, A., Helbing, D., 2000. Congested traffic states in empirical observations and microscopic simulations. Phys. Rev. E 62(2), 1805–1824.
Treiber, M., Kesting, A., 2011. Evidence of convective instability in congested traffic flow: a systematic empirical and theoretical investigation. Transport. Res. Part B: Methodol. 45 (9), 1362–1377.
Van Arem, B., Van Driel, C.J., Visser, R., 2006. The impact of cooperative adaptive cruise control on traffic-flow characteristics. IEEE Trans. Intell. Transport. Syst. 7 (4).
VanderWerf, J., Shladover, S., Kourjanskaia, N., Miller, M., Kishnan, H., 2001. Modeling effects of driver control assistance systems on traffic. Transport. Res. Rec.: J. Transport. Res. Board 1748, 167–174.
Wang, M., Daamen, W., Hoogendoorn, S.P., van Arem, B., 2014a. Rolling horizon control framework for driver assistance systems. Part I: Mathematical formulation and non-cooperative systems. Transport. Res. Part C: Emerg. Technol. 40, 271–289.
Wang, M., Daamen, W., Hoogendoorn, S.P., van Arem, B., 2014b. Rolling horizon control framework for driver assistance systems. Part II: Cooperative sensing and cooperative control. Transport. Res. Part C: Emerg. Technol. 40, 290–311.
Wang, M., Daamen, W., Hoogendoorn, S.P., Van Arem, B., 2016. Connected variable speed limits control and car-following control with vehicle-infrastructure communication to resolve stop-and-go waves. J. Intell. Transport. Syst. 20 (6), 559–572.
Wilmink, I.R., Klunder, G.A., Van Arem, B., 2007. Traffic Flow Effects of Integrated Full-Range Speed Assistance (IRSA). In: 2017 IEEE Intelligent Vehicles Symposium.
Xiao, L., Wang, M., Schakel, W., van Arem, B., 2018. Unravelling effects of cooperative adaptive cruise control deactivation on traffic flow characteristics at merging bottlenecks. Transport. Res. Part C: Emerg. Technol. 96, 380–397.
Xing, J., Muramatsu, E., Harayama, T., 2014. Balance lane use with vms to mitigate motorway traffic congestion. Int. J. Intell. Transport. Syst. Res. 12, 26–35.
Yeo, H., Skabardonis, A., Halkias, J., Colyar, J., Alexiadis, V., 2008. Oversaturated freeway flow algorithm for use in next generation simulation. Transport. Res. Rec.: J. Transport. Res. Board (2088), 68–79.
Yoshizawa, R., Shiomi, Y., Uno, N., Iida, K., Yamaguchi, M., 2012. Analysis of car-following behavior on sag and curve sections at intercity expressways with driving simulator. Int. J. Intell. Transport. Syst. Res. 10 (2), 56–65.
Yuan, K., Laval, J., Knoop, V.L., Jiang, R., Hoogendoorn, S.P., 2018. A geometric brownian motion car-following model: towards a better understanding of capacity drop. Transportmet. B: Transport Dyn. 1–13.
Zheng, Z., Ahn, S., Chen, D., Laval, J., 2011. Freeway traffic oscillations: microscopic analysis of formations and propagations using wavelet transform. Transport. Res. Part B: Methodol. 45 (9), 1378–1388.